Wireless Power Transfer

cambridge.org/wptcup

Controlling wireless power transfer by tuning and detuning resonance of telemetric devices for rodents

Basem M. Badr[1], Art Makosinski[1], Nikolai Dechev[1] and Kerry R. Delaney[2]

[1]Department of Mechanical Engineering, University of Victoria, Victoria, BC, V8W 2Y2, Canada and [2]Department of Biology, University of Victoria, Victoria, BC, V8W 2Y2, Canada

Research Article

Cite this article: Badr BM, Makosinski A, Dechev N, Delaney KR (2020). Controlling wireless power transfer by tuning and detuning resonance of telemetric devices for rodents. *Wireless Power Transfer* **7**, 19–32. https://doi.org/10.1017/wpt.2020.1

Received: 25 August 2019
Revised: 15 December 2019
Accepted: 30 December 2019
First published online: 7 February 2020

Key words:
Biomedical applications; resonance control; rodent; telemetric devices; wireless power transfer

Author for correspondence:
Basem M. Badr, Department of Mechanical Engineering, University of Victoria, Victoria, BC, V8W 2Y2, Canada. E-mail: bbadr@uvic.ca

Abstract

Telemetry acquisition from rodents is important in biomedical research, where rodent behavior data is used to study disease models. Telemetry devices for such data acquisition require a long-term powering method. Wireless power transfer (WPT) via magnetic resonant coupling can provide continuous power to multiple small telemetric devices. Our loosely coupled WPT (LCWPT) system consists of a stationary primary coil and multiple freely moving secondary coils. Our previous LCWPT system was designed to transfer reasonable power to secondary coils at poor orientations but transfers excessively high amounts of power at favorable orientations. Reasonable power is needed for telemetry and radio electronics, but highly induced voltage on the secondary coil creates excess energy which must be dissipated by previous devices, and caused problems (localized heat damage and variations in component properties) leading to drift in operating frequency. To remedy these two problems, a novel scheme is proposed to automatically tune or detune the resonant frequency of the secondary circuit. Our closed-loop controlled tuning or detuning (CTD) approach can be used to prevent excessive power transfer by detuning, or to improve power transfer by tuning, depending on the need. Furthermore, this novel CTD scheme facilitates the use of multiple telemetric devices.

Introduction

Implantable biomedical devices have a significant role in modern medicine and can be used for variety applications. These applications include: real time monitoring of bio-signals of the patient/body, generating stimulus signals, bioelectric recording, and communicating internal vital signs to the outer world. Providing power to these biomedical devices for long-term operation is a challenging task [1–3]. In our application, the telemetric device would record the neural electroencephalographic (EEG) activity of a laboratory rodent [3–5].

Traditional approaches to power telemetric devices use batteries. In the case of implantable telemetric devices, batteries are placed inside the body within the implant, or a transcutaneous wire-based power supply is used. However, the use of wire links to power implantable devices in rodents has a number of difficulties: wire breakage, failure of head-mounted connectors, restriction of normal movement of rodents, the possibility of infection via the wire, and interference from electrical noise sources [4–6]. In the case of batteries, embedded batteries have limited energy storage and life span [2]. In order to avoid the aforementioned problems, wireless power transfer (WPT) is recommended for applications involving rodents for long duration experiments [3–5].

A common characteristic of WPT systems for rodent telemetry applications is loose coupling between the primary and secondary coils [3]. These systems are referred to as loosely coupled WPT (LCWPT), where their coupling coefficient is typically less than 2% [4]. This can be considered as a low efficiency of power transfer for LCWPT systems. Therefore, nearly all WPT systems use magnetic resonant coupling between the primary and secondary coils, to increase WPT efficiency. The magnetic resonant power transfer depends on the frequency match between the inherent resonant frequency of the primary circuit, and the inherent resonant frequency of the secondary circuit [3].

In our application, we use LCWPT to power telemetric devices intended for implant into freely moving small rodents. Our telemetric device is called the rodent implant device (RID), which functions as a stimulator and EEG sensor. The RID prototype would be suitable for subcutaneous implantation in a rat, or would be suitable as a head-mounted device for a mouse. Figure 1 illustrates a freely moving mouse in an animal cage encircled by a primary coil, where the telemetric device would be placed on a mouse's head. The volume within the primary coil is $250 \times 120 \times 45$ mm^3 (length × width × height), and the cage volume is $250 \times 120 \times 150$ mm^3 (length × width × height). This cage size is needed to meet the minimum animal care standards for mice [3–5].

© Cambridge University Press 2020

CAMBRIDGE UNIVERSITY PRESS

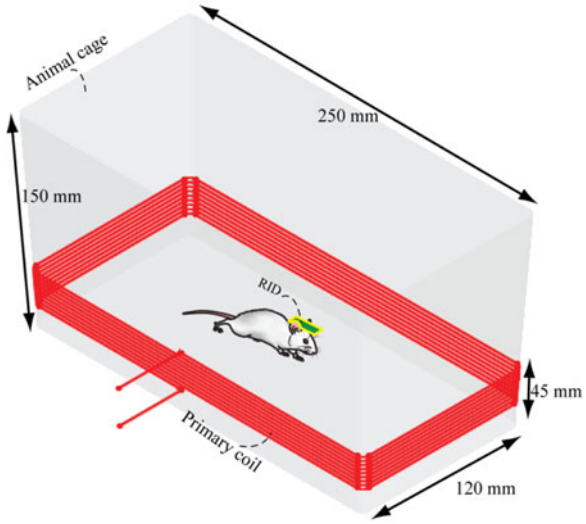

Fig. 1. WPT concept for a mouse, with primary coil wrapped around a small mouse housing cage.

There are some problems that may cause a resonant frequency mismatch in a WPT system. These problems are: (1) the loading effect, where McCormick *et al.* reported the loading effect causes mismatch of the resonant frequency of the WPT systems [7]. (2) The temperature effect, where Wang *et al.* found that highly induced voltage generates higher temperatures in the implant that affects the secondary capacitor (C_s) and creates the resonant frequency mismatch of the L_SC_S-tank circuit [8]. Also, device electronics must be protected from excessively highly induced voltage, which must be dumped as heat via voltage regulators. This leads to significant localized heat in the implant that may damage the electronic components of the telemetric devices. (3) In the case of multiple secondary circuits within the same primary coil, mutual coupling may develop between the secondary coils. This mutual coupling will cause mismatch of the resonant frequency of each secondary circuit [9]. (4) The effect of the reflected impedance from the secondary circuit over the primary circuit, where the reflected impedance causes a shift in the resonant frequency of the primary circuit [9, 10].

This paper provides a novel scheme to detune (or tune) the resonant frequency of the secondary tank circuit of the telemetric device. This is done by using a microcontroller (MCU) located on-board the telemetric device to monitor its own received power and to tune or detune its resonant frequency as needed. Furthermore, this novel scheme allows for the use of multiple telemetric devices to operate within a single primary coil, since each secondary circuit can tune or detune its resonant frequency independently of the others. This allows for applications where multiple rodents (each equipped with a telemetric device) can run around in a single primary coil, all receiving adequate power to power their telemetric device regardless of the rodents' position or orientation within the cage.

This paper is organized as follows. Section "Introduction" provides the research motivation of using a WPT system for telemetric devices for rodents and the issues of using multiple secondary coils in the same primary coil. Section "Literature survey" cites the literature regarding resonant frequency mismatch in the WPT systems. Section "Limitations of other approaches in the literature" explains limitations of previous research. The methodology of our controllable LCWPT system is described in Section "Methodology for control of tuning or detuning." Section "LCWPT theory" describes LCWPT theory. The design of the proposed controllable LCWPT system is reported in Section "Development and design of proposed CTD system." The experimental setup of our controllable LCWPT is shown in Section "Experimental setup of the CTD LCWPT hardware." The experimental results of our controllable LCWPT are reported in Section "Experimental results with the CTD LCWPT system." Section "Conclusion" reports the experimental results of using multiple RIDs in the same cage (primary coil). A discussion of the results is provided in Section "Discussion", and the conclusion in Section "Conclusion."

Literature survey

A number of researchers have investigated WPT systems employing magnetic resonant coupling. These WPT systems were intended for either large-scale applications (received power higher than 10 W) or small-scale applications (received power lower than 10 W). The literature shows that the transferred power can be controlled by changing the resonant frequency between primary and secondary coils, or by using power converters in the secondary receiver circuits to control the power flow to the application load [10–12]. There are two main approaches to control the magnetic resonant coupling in WPT systems, which are: (1) to control the resonant frequency of the primary circuit, or (2) to control the resonant frequency of the secondary circuit.

Given our objective to have multiple rodents with telemetric devices in a single cage, the control scheme to control the primary circuit resonance is not suitable. If there are multiple secondary coils in a single primary coil, each secondary circuit may have a slightly different resonant frequency that may vary in time due to various factors. The resonant frequency of each secondary circuit may shift as a result of the mutual inductance effect between the coils, and possible heating effects that change capacitance or inductance properties. The literature shows these limitations of controlling the primary circuit resonance [13–16]. Hence, by controlling the resonance of the primary circuit, all the secondary circuits cannot maintain resonance with it. In contrast, it is preferable to control the resonant frequency of each secondary circuit and fix the resonant frequency of the primary circuit. Another limitation of tuning/detuning the primary circuit is the use of continuous switching, which can cause a large power loss due to switching, and the resultant surge currents that can damage the switching devices [10]. This section will focus on the literature search with regard to controlling the resonant frequency of the secondary circuit of WPT systems.

With regard to approaches of controlling the secondary coil resonance: James *et al.* used a variable inductor circuit within the secondary LC-tank, which consists of a tuning inductor (L_2), two switches, two diodes, and a compensating capacitor (C_2). The two switches were controlled by a phase lock loop (PLL) scheme. The variable inductor circuit was connected in parallel with the LC-tank, where the current through L_2 was balanced by the current through C_2 for normal operation. The PLL controlled the resonance of the secondary circuit, when the current through L_2 changed (increased/decreased). Their variable inductor circuit kept the resonance of the secondary circuit by varying the current in the tuning inductor (L_2) and the compensating capacitor (C_2) [17]. Si *et al.* designed a tuning/detuning (DTD) control technique that dynamically changed the tuning/detuning condition of the secondary circuit with respect to the required voltage to power the load (application device). This

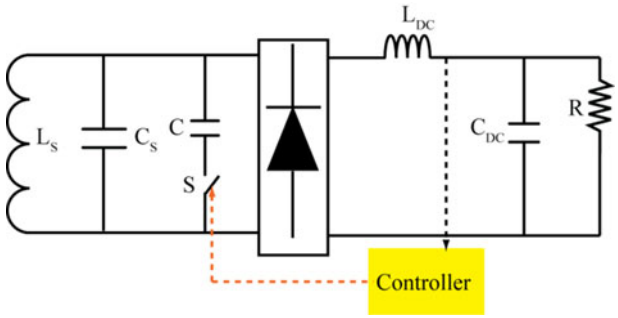

Fig. 2. Schematic of the DTD technique.

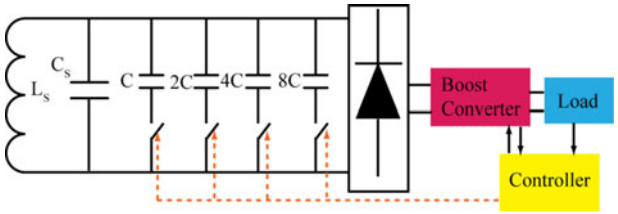

Fig. 3. Schematic using relay to tune the secondary circuit.

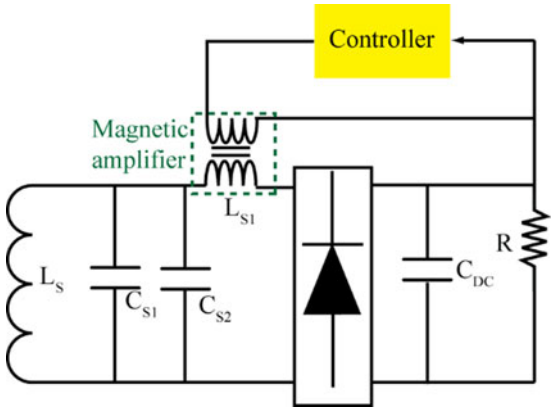

Fig. 4. Using magnetic amplifier in the secondary circuit.

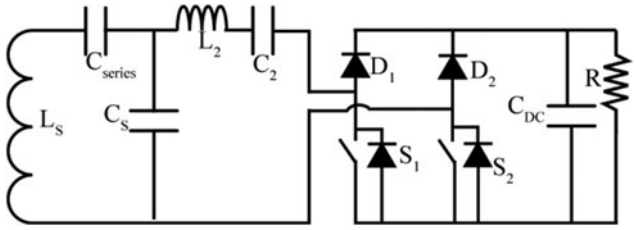

Fig. 5. Using fast switching in the secondary circuit.

was achieved by deliberately putting a soft switched capacitor (C) parallel to the secondary capacitor (C_s), as shown in Fig. 2. The output voltage was used as a feedback signal to determine the turn on/off time of the soft switch to achieve the required equivalent capacitance. The DTD process was divided into four segments: initial, discharging, charging, and final. Based on analytical analysis of each segment, an iterative method was used to obtain a numerical solution for the detuned operating frequency [18]. There are some challenges with the DTD method, as follows: the relationship between the tuning capacitance and the output voltage is bell shaped; therefore, it can result in two possible operating points with one being in the over-tuning region and the other in under-tuning region [19]. It is insufficient to use the DTD method to achieve maximum power transfer, when the operating frequency shifts to the other region due to circuit parameter variations. It may track in the wrong direction and fail to control the output voltage [20]. Covic *et al.* built a self-tuning WPT system. They used a binary series of capacitors (C, $2C$, $4C$, and $8C$) that were switched via relays wired across the secondary LC-tank (L_SC_S), as shown in Fig. 3. The binary series capacitors were added to tune the secondary LC-tank. The equivalent capacitance value from adding the tuning capacitors is big, in the range of μF which is suitable for high power applications. Their WPT system was used in material handling applications that require 500 W [21]. Hsu *et al.* designed a system using an inductor–capacitor–inductor (LCL) that was based on a magnetic amplifier in the secondary circuit, as shown in Fig. 4 [19]. Hsu *et al.* discovered that their control approach (LCL) was restrained by the tuning step. A larger step change in the inductance often caused chattering of the output voltage. Although the chattering effect could be reduced by using a smaller step change in the inductance, it caused the overall response to be sluggish. They remedied this problem by designing a fuzzy controller to make the overall response fast [20].

Huang *et al.* designed a fast switching control topology to regulate the power flow by adjusting the equivalent alternating current (AC) output voltage of the LCL network using two diodes and two switches (S_1 and S_2) in the secondary circuit. Their WPT system was used for vehicle application, where the received power of the secondary circuit was 2.5 kW. The idea of their topology is similar to the traditional controlled rectifier to regulate the average output current through the rectifier, while allowing variance in mutual coupling. Figure 5 shows their designed secondary circuit, the series tuning capacitor (C_{series}) and C_S are used to achieve the resonance of the secondary circuit, the values of L_2 and C_2 are designed to accommodate the extra inductance introduced by the nonlinear effect of the rectifier to minimize the current in the secondary coil (L_S) [22]. Hsu *et al.* used the DTD control technique that was designed by Si *et al.* in [18], where the switch was connected in series with a tuning/detuning capacitor that are connected in parallel with the secondary LC-tank circuit, as shown in Fig. 2. The objective of their approach was to control the power flow of the LC-tank circuit by either increasing or decreasing the tuning/detuning capacitance. The value of the tuning/detuning capacitor is big, in the μF range. The generated signal from the controller is denoted as a switching signal that controlled the effective tuning/detuning capacitance using different values of the duty cycle. The switch signal controlled the charging and discharging of the capacitor (can either be a unidirectional or bidirectional switch). They used a Proportional-integral (PI) controller [23], however, the PI controller was incapable of performing control over a bell-shaped relationship between the tuning/detuning capacitance and the induced voltage, and the chattering effect, as explained in [24]. The performance of the controller was dependent on two major factors: the tuning/detuning step-size and the sampling frequency. Therefore, they used a fuzzy logic controller to overcome the limitations of the PI controller and make the system response fast [21]. The WPT systems designed by Hsu *et al.* [19, 20, 23, 24] are used for vehicle applications.

Although the presented research of Hsu *et al.* was able to overcome the drawbacks of the previous solutions, some issues

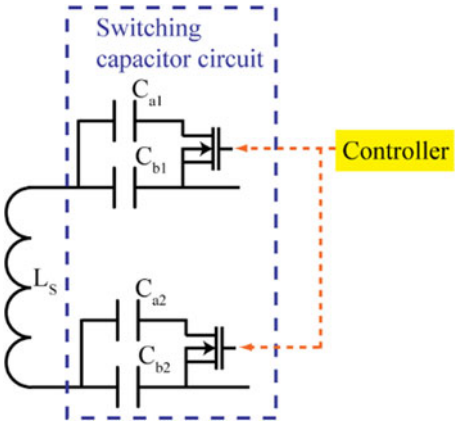

Fig. 6. Designed switching capacitors of [26].

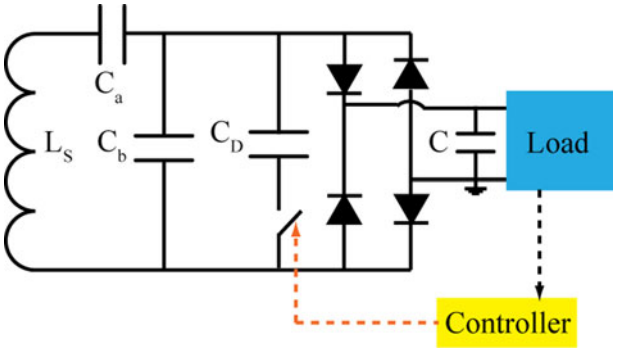

Fig. 7. Controlling open circuit impedance of the secondary circuit.

remain. Namely, the nonlinearity, the slow dynamic, and the bulkiness of the magnetic amplifier as the variable inductors are significant limitations of the proposed approach. Also, their design depended on a complicated control algorithm using fuzzy logic for the selection of a sampling frequency and step size [25].

Petersen designed a tuning WPT for biomedical applications, with efficiency of 0.7%. He used a switching capacitor circuit that was switched by metal–oxide–semiconductor field-effect transistors (MOSFETs) to change the capacitance of the secondary circuit, as shown in Fig. 6. The switched capacitors C_{a1}/C_{a2} are small with respect to un-switched capacitors C_{b1}/C_{b2}, while the effective range of the variability was small, and vice versa. The controller was used to switch the MOSFETs and control the timing of the MOSFET switching using different values of duty cycles. The controlling of the timing on the MOSFET switching allowed a continuously variable capacitance, where the minimum capacitance occurs with 50% duty cycle, and the maximum capacitance occurs with 100% duty cycle [26]. Riehl *et al.* designed a resonant WPT that used parallel series resonant secondary capacitors (C_a and C_b) with an open-circuit impedance (Z_{oc}) adjustment, by a switching capacitor (C_D), as shown in Fig. 7. The capacitor (C_D) was switched to adjust the open-circuit (Z_{oc}) to reduce the induced voltage. The switching capacitor changed the open-circuit impedance (Z_{oc}) that also changed the reflected impedance seen by the primary coil, so the switching capacitor regulated the induced voltage [27].

Another alternative way to control the voltage induced in the secondary coil circuit is using power electronics. However, in this approach the heat is still dissipated in the secondary circuit, since the magnetic resonant coupling remains [10, 11]. Examples of this approach include: Yung-Chih *et al.* designed multiple wireless power receivers using a programmable power path. Their system depended on a linear low dropout regulator (LDO), where the LDO input voltage (rectified voltage) is controlled very close to the LDO output voltage. The rectifier voltage can be higher than the regulator output that made the power transfer very inefficient through the LDO. Therefore, a switching mode regulator was applied for better efficiency when the voltage step down ratio is large [28].

Limitations of other approaches in the literature

The control schemes described for tuning/detuning the secondary circuit in [17, 19–24, 27, 28] are more suitable for WPT systems for large-scale applications like wireless charging of vehicles. This is because much higher power transfer levels are involved. In this case, the needed tuning/detuning inductor occupies a large volume, and the tuning/detuning capacitor values are large, in the range of μF. The control schemes of the secondary circuits in [19, 20] are complicated and have a slow dynamic response when tuning/detuning secondary circuits, which causes a sluggish response [25], and would not be suitable for fast application devices (such as the RID on fast moving rodents). The limitation of using the DTD method [20] is that any change in the parameters of the secondary circuit affects the operation of the four segments and creates a resonant frequency mismatch. The designed WPT using relays [21] is not suitable for small-sized biomedical implant applications, since the relay occupies a large volume. Also, the relay requires a high operating current to turn on, which represents a problem for low power applications such as our RID telemetry devices. Petersen claimed that his WPT system was used for biomedical applications [26]; however, the maximum received power of his controlled secondary circuit (Fig. 6) was 15 W, which is considered high power for implant applications. Also, Petersen's WPT system was AC–AC, where the input to the primary circuit was AC power, and the received power at the secondary circuit was AC power. Since there was no rectification on their secondary circuit, direct current (DC) power was not available, which prevented the use of digital electronics needed for telemetry acquisition, signal processing, and digital communication. The WPT system of Riehl *et al.* (Fig. 7) [27] depended on controlling the reflected impedance of the secondary circuit seen by the primary circuit. Their WPT system was suitable for large WPT applications that have high coupling coefficient but their WPT system is not suitable for small WPT applications, such as LCWPT systems for biomedical devices. This is due to the reflected impedance of the secondary circuit, which is a function of the coupling coefficient, which can be neglected in LCWPT systems, as written in equations (1) and (2). Also, their designed secondary circuit likely has a floating gate drive problem because of the connection of the switching capacitor (C_D) with the full bridge rectifier, as is explained in detail in our Section "Development and design of proposed CTD system."

Methodology for control of tuning or detuning

In the previous sections, we reviewed two main approaches to adjust the magnetic resonant coupling between the primary circuit and the secondary circuit(s) of WPT systems. These are:

(1) controlling the resonance of the primary tank circuit, or (2) controlling the resonance of the secondary tank circuits. Our proposed LCWPT system is based on the second approach, whereby the resonant frequency of the secondary circuit(s) is tuned/detuned in order to match them with the fixed resonant frequency of the primary circuit.

In using the second approach, there are two possible modes: (i) tuning the secondary circuit to maintain magnetic resonant coupling with the primary circuit, or (ii) detuning the secondary circuit to reduce the magnetic resonant coupling with the primary circuit. Tuning the magnetic resonant coupling will be used when resonant frequency mismatch occurs such as from mutual coupling effects from multiple RIDs, or from poor orientation between the secondary coil and primary coil. Detuning the magnetic resonant coupling will be used in cases where good orientation between the secondary coil and the primary coil leads to too much capture of magnetic flux. Without the proposed closed loop-controlled tuning or detuning (CTD) system, this excessive capture of magnetic flux will generate a high voltage in the secondary circuit, which must be controlled by other means, such as regulators. This would lead to significant localized heat in the implant. If the proposed CTD system is employed, the induced voltage on the RID can be limited to a specified voltage by design, as shown in Section "Development and design of proposed CTD system" and "Experimental setup of the CTD LCWPT hardware."

The CTD LCWPT secondary circuit configuration employs four ferrite rods placed at the inside corners of the secondary coil [3]. The diameter and length of the ferrite rods is 1.6 and 8.6 mm, respectively, whereas the secondary coil size is 22 mm × 14 mm^2. This configuration is denoted as 4MF (four medium ferrites), which improves the WPT when the secondary circuit plane is oriented at various angles with respect to the primary coil. We have used the 4MF configuration in this work, using our new CTD L_SC_S-tank circuit, where this system is collectively called the RID.

A number of experiments were done to validate the proposed RID. One experiment was done to investigate the power transfer for various orientations of the RID with respect to the primary coil. Another experiment was done to characterize the quality curve (received power versus frequency) of the RID, by adding and removing capacitors within the L_SC_S-tank circuit. This helped to establish the relationship between the capacitor values needed to tune or detune the RID operating (resonant) frequency by specific amounts. Another experiment was done to determine the utility of using a MOSFET based switching system within the L_SC_S-tank of the RID, while it operates within the primary electromagnetic field.

LCWPT theory

Inductive power transfer (IPT) is a popular technique for WPT over a near-field region (short range). This technique is based on two fundamental laws: Ampere's law and Faraday's law. IPT is based on the changing magnetic field that is generated due to alternating currents through a primary coil. The alternating magnetic field induces a voltage onto a secondary coil [3–5, 29].

There are four topologies for achieving magnetic resonant coupling between the primary and the secondary coil. The topologies are SS, SP, PP, and PS, where the first S or P stands for series or parallel compensation of the primary winding, and the second S or P stands for series or parallel compensation of the secondary winding [3]. For this work, our proposed CTD system uses the SP topology. It is highly suitable for LCWPT systems, such as biomedical applications, because it provides suitable power to the application load, and reduces the reflected impedance problem [10, 29]. Figure 8(a) shows the SP topology used in this work.

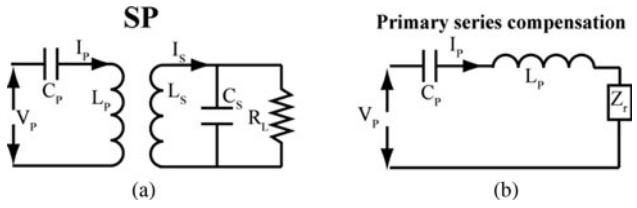

Fig. 8. SP topology of primary and secondary coils: (a) SP topology and (b) primary series compensation.

The loading effect of a secondary coil back onto the primary circuit is shown in Fig. 8(b), as a reflected impedance Z_r. It depends on the coupling factor and operating frequency, and it can be written as [10]:

$$Z_r = \frac{w^2M^2\ R_L}{R_L^2(w^2C_sL_s-1)^2+w^2L_s^2} + j\ \frac{-w^3M^2\ [R_L^2C_s\ (w^2C_sL_s-1)+L_s]}{R_L^2(w^2C_sL_s-1)^2+w^2L_s^2} \quad (1)$$

where, w is the radian operating frequency, R_L is the load resistance, L_S is the secondary coil and C_S is the secondary capacitor, M is the mutual inductance between the primary and secondary coils, and k is the coupling coefficient (value between 0 and 1).

In order to minimize the VA ratings of the power supply and to achieve magnetic resonant coupling, it is desirable to operate at the zero-phase angle of the impedance at the resonant frequency of the load impedance. This zero-phase angle of the impedance at the resonant frequency must be achieved to ensure maximum power transfer. The primary capacitance used for SP topology is obtained by [10]:

$$C_P = \frac{1}{w^2\left(\frac{L_P-M^2}{L_S}\right)} \quad (2)$$

The maximum power received by the secondary occurs when the load is conjugately matched. At magnetic resonance, the reactive components cancel, and the impedance is simply the real component, which is the resistive loss of the secondary tank (R). For maximum power transfer to occur, the load resistance needs to be equal to the resistive loss of the secondary tank.

Development and design of proposed CTD system

The resonant frequency of the secondary circuit in the RID is a function of the L_SC_S-tank circuit. The proposed controller technique tunes/detunes the resonance of the secondary circuit by adding/removing capacitance in parallel with the secondary capacitor (C_s) to change the overall capacitance value of the L_SC_S-tank circuit. Adding/removing capacitance is achieved by electronic switching MOSFETs connected to physical capacitors within the L_SC_S-tank circuit. There are two different modes of operation achieved by adding/removing capacitance as follows: (1) small-adjustment mode: by adding/removing (via electronic

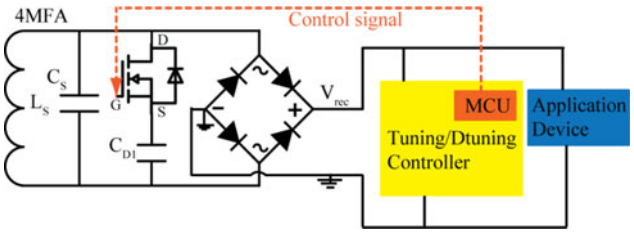

Fig. 9. Initial switching capacitor technique (non-working).

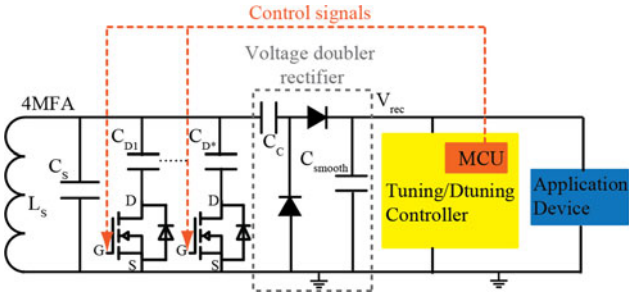

Fig. 10. Switching capacitor technique using a voltage doubler rectifier, whereby the source of the MOSFET is grounded on a common ground.

switching) small capacitor values in the range of 10–70 pF for fine tuning the resonant frequency of the secondary circuit. These small capacitor values help to tune the secondary circuit when the resonant frequency deviates due to the mutual coupling effect from the multiple secondary circuits, or due to the heating effect. (2) Big-adjustment detune mode: by adding/removing (via electronic switching) large capacitor values in the range of 100–800 pF to detune the RID when excessively highly induced voltage is gathered by the telemetric device, due to favorable orientation between the primary and secondary coils. Experiments were done with different secondary circuit prototypes to determine the appropriate capacitor values corresponding to appropriate shifts in resonant frequency, as explained in the next section. The main features of these capacitors are high Q and low effective series resistance (ESR), where the dielectric material is ideally independent of temperature and its voltage coefficient is constant over different applied voltages.

We designed our secondary coil (L_S) with a high quality factor (Q), which is shown by the peak curve as shown in Fig. 13(b). The high Q coil gives a narrow frequency band which makes the secondary circuit sensitive to the operating frequency of the primary circuit. The resonant frequency (w_{res}) and the quality factor (Q_S) of the secondary circuit, using parallel compensation, are defined as [30]:

$$w_{res} = \frac{1}{\sqrt{L_S C_S}} \tag{3}$$

$$Q_S = \frac{R_{AC}}{w_{res} L_S} = w_{res} C_S R_{AC} \tag{4}$$

where R_{AC} is the equivalent resistance that corresponds to the real power delivered to the secondary application load. The secondary application load is the collection of all application circuits (i.e. MCU, radio, etc.) on the secondary that consume power. The increasing heat may affect the capacitance C_S of the $L_S C_S$-tank depending on the dielectric material of the capacitors [31, 32], leading to resonant frequency shift.

Initial designs

As we carried out this work, we tried a few different secondary circuit configurations to tune/detune the resonance of the RID in a controllable manner. Some of these initial configurations do not work well, and we have decided to describe them here briefly as a point of reference to explain why they don't work.

As explained in the methodology, we want to be able to add or remove capacitance within the $L_S C_S$-tank, upon command. We used MOSFETs to switch open/close a set of capacitors (C_{D1}) that are in parallel to C_S, as shown in Fig. 9. Our initial (non-working) configuration contains the $L_S C_S$-tank, the switching elements (MOSFETS), a set of capacitors, a full-wave rectifier bridge, the secondary application load, and a tuning/detuning controller (an on-board MCU with code and a circuit that measures the rectified voltage (V_{rec}) and controls the switching elements). We used a Nordic MCU (nRF24LE1-F16Q24) that is suitable for ultra-low power applications [33].

The configuration shown in Fig. 9 does not work, because it has a floating gate drive, where the $L_S C_S$-tank is AC (V_{ind} sinusoidal), while the MCU and application load are DC. Note the MOSFET is connected in series with the tuning/detuning capacitor (C_{D1}), where both are connected in parallel with C_S. The problem occurs because we cannot connect the DC logic signal of the MCU, to the AC conditions present at the source of the MOSFET. Under these conditions, the voltage at the source of the MOSFET is sinusoidal and therefore V_{GS} will be floating with respect to the gate threshold voltage ($V_{GS(th)}$). This creates a floating gate problem, causing erratic operation of the MOSFETs. In order to overcome this problem, we designed the working solution shown in Fig. 10. Here we decided to use a voltage doubler rectifier circuit between the AC side and the DC side of the secondary circuit, which provides a common ground for both sides. Using a voltage doubler rectifier is very unusual for the rectification of AC power, since it has a lower efficiency than full-wave bridge rectifiers, and nearly all other systems do not use it. The voltage doubler rectifier consists of two diodes, a coupling capacitor ($C_C = 0.1\ \mu F$), and a smoothing capacitor ($C_{smooth} = 0.1\ \mu F$). This configuration avoids the floating gate problem, whereby the tuning/detuning capacitors are connected to the drain of MOSFETs, as described in the next section.

An alternative way to eliminate the floating gate drive problem is to use isolating gate drives. However, isolated gate drives need a separate power source, and they will occupy more size on the secondary circuit. In our application, the PCB of the RID is limited in size because of the application constraint for use with rodents and for implantable medical applications. Another possible alternative is to use an integrated circuit (IC) array of capacitors for increased resolution for tuning/detuning. However, most IC capacitor arrays are CMOS and cannot handle voltages above 18 V, and may have high switching losses [10].

Working design of CTD system

For the working CTD system, we use MOSFETs to switch open/close capacitors (C_{D1}, C_{D2}, and C_{D*}) that are in parallel to C_S, as shown in Fig. 10. The source of the MOSFETs is connected to the common ground, which assures the source voltage (V_S) is zero,

allowing the control signal (gate voltage, V_G) from the MCU to effectively switch the MOSFET on/off. This is not intuitive, since it must use the voltage doubler rectifier between the AC and DC side of the circuit, to operate the MOSFETs via a logic control signal from the MCU, since a common ground exists.

The theory of operation of our proposed working system is now described: for achieving maximum power transfer, the resonant frequency of the secondary circuit (telemetric device) must equal the operating frequency of the primary circuit (1 MHz in our application). As previously explained, the resonant frequency of the secondary circuit may increase because of the heating effect [8, 31], which causes the secondary capacitor (C_S) value to drop. In addition, the resonant frequency of the secondary circuit may decrease when the secondary inductance (L_S) increases because of the mutual coupling of multiple secondary circuits [8, 34, 35] within the primary field. In the case of the inductance change, the increasing inductance can be denoted as ΔL, where the equivalent secondary inductance (L_{eq}) due to the multiple secondary coils, is given as:

$$L_{eq} = \Delta L + L_S \tag{5}$$

As result of the multiple secondary circuits/RIDs, the total reflected impedance (Z_{rtot}) from the multiple RIDs is given as [35]:

$$Z_{rtot} = \sum_{i=1}^{n} Z_{ri} = n\frac{W^2M^2}{Z_s} \tag{6}$$

where n is the number of the RIDs in the cage. The equivalent mutual inductance and coupling coefficient of the multiple RIDs are [35]:

$$M_n = \sqrt{n}M, k_n = \sqrt{n}k \tag{7}$$

In order to compensate the ΔL, the secondary capacitance should be:

$$C_S = \frac{1}{w^2(L_S + \Delta L)} \tag{8}$$

Therefore, equation (8) provides a theoretical way to determine the amount of corrective capacitance needed to account for an inductive change of ΔL. Since there may be various operational scenarios, the required value of C_s to maintain resonance will be different for various scenarios. Therefore, in our proposed technique, we employ multiple capacitors (C_{D1}, C_{D2}, and C_{D^*}) to tune or detune the resonant frequency of the RID for various scenarios. From experimental testing with our working RID described here, the received power of the secondary circuit versus frequency (see Fig. 13(a)) is represented by a bell-shaped curve. Consider the peak in Fig. 13(a), along with the region to the right and to the left of the peak. The right region represents an over tuning region where the secondary circuit has a frequency higher than the resonant frequency (1 MHz). The left region represents an under tuning region where the secondary circuit has a frequency lower than the resonant frequency (1 MHz). For the CTD system, the L_SC_S-tank has been designed to startup (begin operation) in the over tuning region. Recall that if startup occurs in an ideal orientation (secondary coil plane and primary coil plane are parallel), and also if our telemetric device frequency is tuned exactly to the primary circuit frequency, too much power will be transferred causing excessive heat and possibly damage. As a result, the telemetric device starts up out of tune in the over tuning region. If the MCU senses that more power transfer is needed, it will begin to drop the total tank capacitance C_s, by adding capacitors in parallel to C_s, and thereby better tune the secondary frequency to the primary frequency. In the poor orientations, the control system will try to exactly match the secondary circuit frequency to the primary circuit frequency. More information about the process to tune and detune the secondary circuits by adding/removing capacitors (C_{D1}, C_{D2}, and C_D) is described in Section "Experimental results with the CTD LCWPT system." While switching on and off between the capacitors (C_{D^*}) we must keep the value of the R_{AC} almost the same, to achieve the matched impedance (R_L) and avoid the reflected impedance problem that may detune the resonance of the primary circuit, as reported in [28]. The resistance, R_{AC}, should maintain its value during switching as [25, 35–37]:

$$R_{AC} \approx R_P\frac{\pi^2}{8} \tag{9}$$

where R_P is the equivalent parallel resistance of the secondary coil, and is measured using a LCR meter [33–35]. Control of the RID telemetry device is based upon a system on chip (SoC) from a Nordic Semiconductor (nRF24LE1). This SoC includes a 2.4 GHz RF transceiver core, embedded Flash memory (16 kB), and a set of on-chip analog and digital peripherals which provides a flexible, single chip solution for our application [33]. The rectified voltage (V_{rec}) is measured by the 12-bit analog to digital converter (ADC) of the SoC. The 2.4 GHz radio provides a wireless link to the base station which passes the transmitted data on to the laptop for view/saving the data. The lack of memory precludes storage of parameters such as sample frequency, gain settings, and stimulation parameters. The sampling frequency of the CTD system is selected based on the settling time (t_S). The settling time can be written as [32]:

$$t_s = R_{AC}C_{D*} \tag{10}$$

The sampling time of the controller must be higher than t_S, otherwise the controller response will be sluggish with high values of the R_{AC} and C_{D^*} [32]. The power requirements for the RID telemetric device increase linearly with the frequency of sampling of biological data. The time constant of our system is based on the sampling rate/number of samples per packet. We set the sampling frequency of our RID at 409 Hz and 14 samples per packet, so the data is transmitted at 29.2 Hz or 34.2 ms per point.

Experimental setup of the CTD LCWPT hardware

Our complete CTD LCWPT system is described as two circuits, namely the primary circuit and the secondary circuit, as illustrated in Fig. 11. The SP topology is used to achieve magnetic resonant coupling between the primary circuit and the secondary circuits as described in Section "LCWPT theory." A DC power supply (V_{CC}) is used to power the primary circuit. A signal generator (Agilent 33250A) provides a square signal wave (V_G, duty cycle 0.5) at 1 MHz to a gate driver (MIC4421) [38] to drive a MOSFET (IRF840) [39] in a Class-E power amplifier. The Class-E amplifier is used to generate a sinusoidal current (I_P) to

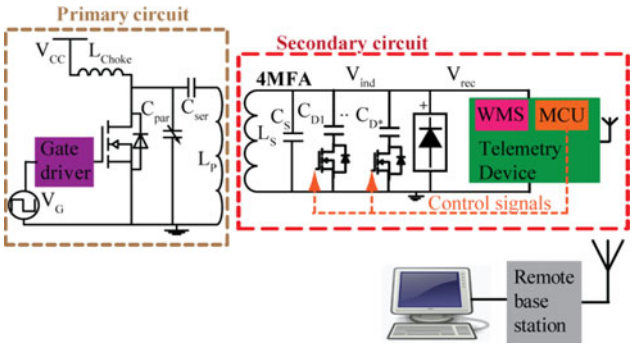

Fig. 11. Block diagram of our CTD LCWPT system.

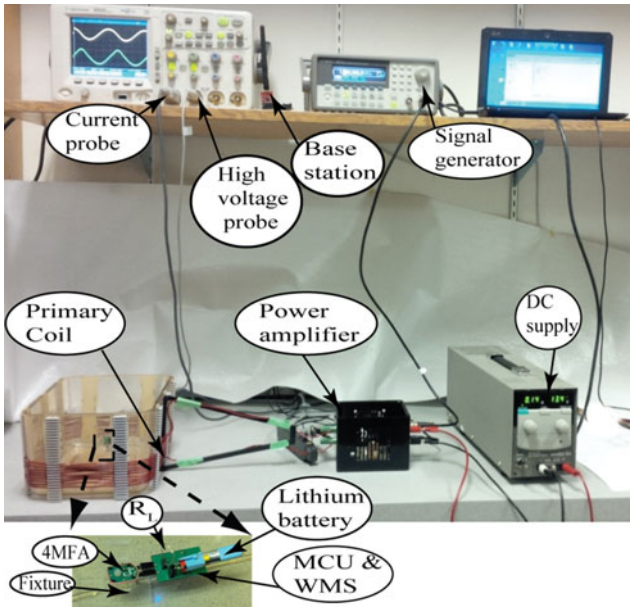

Fig. 12. Experimental setup of our controllable LCWPT system.

Table 1. Parameters of the primary and the secondary coils

Configuration	AWG	R_P (kΩ)	Q	L (μH)
Primary coil (L_P)	22	49.5	165	38.5
Secondary coil (L_S)	44	8.2	55	19.3

the primary coil (L_P). This primary current (I_P) in turn creates an oscillating electromagnetic field. The alternating magnetic field induces a sinusoidal voltage (V_{ind}) in the secondary coil (L_S). This induced voltage is rectified within the RID telemetry device into a DC voltage (V_{rec}) by the voltage doubler circuit. The MCU measures V_{rec} and makes a control decision depending on the measured value V_{rec} and the desired set point voltage value. Using its digital output ports, the MCU switches the MOSFETs on or off as needed for controlling the resonant frequency. This control scheme is closed loop and occurs locally on the telemetric device, with no outside intervention needed. For testing purposes only, we also added a wireless measurement system (WMS), to measure and verify the V_{rec} of any telemetry device under test. The WMS allows us to monitor performance, and it overcomes many problems reported when using corded oscilloscope probes [3–5, 40]. A 2.4 GHz radio communication is built into the WMS platform and uses a proprietary handshaking network protocol to transfer the measured data of the telemetry device to a base station. The WMS is not needed for operation of the RID telemetric device and is only used for testing purposes.

The primary circuit consists of a Class-E amplifier that uses a series compensation topology. The Class-E amplifier can deliver a maximum sinusoidal current (peak-to-peak) of 6 A through the primary coil, however, we use only up to 2 A in this work. The MOSFET (IRF840) used in the amplifier was selected due to its relatively low output capacitance (C_{oss}) at high V_{DS} (drain source voltage of the MODFET) [39]. It is important to note that the C_{oss} is effectively absorbed by C_{par} [3]. Sokal *et al.* demonstrated the operational characteristics of a zero-voltage-switching (ZVS) inverter of the Class-E power amplifier. The ZVS approach is used to identify ideal voltage and current waveforms that minimize switching losses [41–43].

The RID (secondary circuit) contains a L_SC_S-tank, uses ferrite arranged as the 4MF configuration [3], the MOSFETs, the capacitors, the voltage doubler rectifier, the secondary application load, and the SoC (tuning/detuning controller system), as shown in Fig. 14. Two N-channel MOSFETs were used for the switching elements in this design. The properties of these MOSFETs are high power handling (V_{DS} up to 60 V), nanosecond switching (15 ns) capabilities, and low on-resistance (1.4 Ω) that should not damp the coupling factor of the L_SC_S-tank. To build the voltage doubler rectifier, we used diodes which have small reverse current (100 nA) and short reverse recovery time (3 ns).

To achieve high quality factors, inductors with low ESR are required for high frequency operation, due to the coil skin effect and proximity effect. Our desired operational frequency is 1 MHz, to avoid losses due to tissue absorption [3]. To reduce the ESR, multistrand Litz wires are used in our design, and highly recommended [3, 4]. The secondary coil was wrapped around a PCB with 44 AWG Litz wire, and the total coil size is 13.25 × 20.25 × 1.6 mm^3 (length × width × height). The parameters (R_P, Q, and L_s) of primary and secondary coils are measured using a HP 4285A LCR meter and listed in Table 1. The L_SC_S-tank is created by using a 1313 pF capacitor (C_s) to sharply resonate the RID at 1 MHz. A HP 4193A Vector Impedance Meter is used to measure the resonant frequency and impedance of the L_SC_S-tank of the RID, where the measured impedance (R_{LC}) at the resonant frequency was 7.04 kΩ.

The impedance matching within the RIDs has been designed appropriately to avoid internally reflected power loss from the secondary load R_L to the L_SC_S-tank and the primary circuit via the reflected impedance (Z_{rtot}). The maximum power transfer occurs when the resistive component of the load R_L is conjugately matched [1]. Our experimental measurements make use of a conjugately matched load R_L to ensure the maximum power transfer for the overall system. The R_P of the secondary coil (L_S) is 8.2 kΩ, so the R_{AC} is recommended to be kept around 10.2 kΩ, while switching capacitors (C_{D^*}). The used match impedance (R_L) for the experimental measurements is 10 kΩ.

For our controllable LCWPT experiments, the primary coil is wound around a rodent cage (Fig. 1). Figure 12 illustrates the experimental setup of the complete CTD LCWPT system. The output voltage of the Class-E power amplifier is measured by a high voltage probe and the primary current (I_P) is measured by a current probe (Agilent N2893A).

In order to determine the required capacitance values for the switching capacitors to tune/detune the RID, a prior experiment

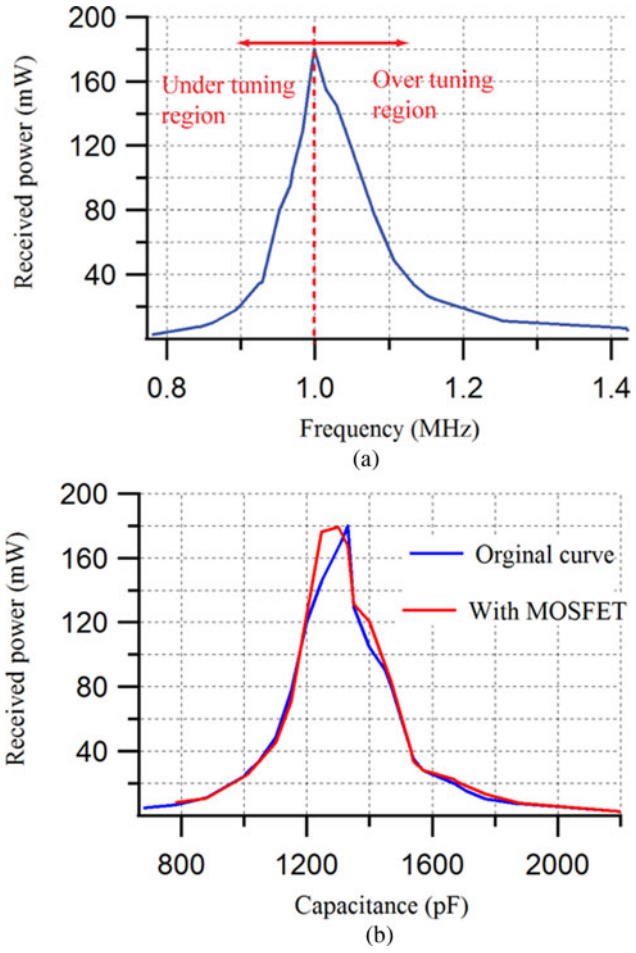

Fig. 13. Received power versus frequency/capacitance: (a) power versus frequency and (b) power versus capacitance with and without MOSFET.

was done to create a received power versus capacitance curve (red curve of Fig. 13(b)). We also used different values of capacitors to alter the total secondary capacitance (C_S), to obtain the curve of the received power versus the frequency/C_S, as shown in Fig. 13(a)/13(b). The curve has a peak received power of 180 mW at the resonant frequency of 1 MHz when using $C_S = 1313$ pF.

We also did experiments to determine the effect of using MOSFETs within the L_SC_S-tank circuit. For reference, the red colored curve of Fig. 13(b) shows the experiments with capacitors only, and no MOSFETs within the L_SC_S-tank. By adding the MOSFETs within the L_SC_S-tank, we noticed there is a difference between the received power versus capacitance, as shown in the blue curve of Fig. 13(b). This difference is due to the stray capacitance of the MOSFET that changes in the electromagnetic field.

We noticed the impedance value of the RID change when we switched with different values of capacitors (C_{D^*}). Therefore, we used a combination of switched capacitors (C_{D^*}), which achieves a constant impedance value of the RID. Moreover, the value of secondary capacitor (C_S) is chosen as lower than 1313 pF, so that upon startup the secondary circuit will be in the over tuning region. Adding/removing capacitance will give us the ability to move the secondary resonance to the operating point and the under-tuning region, or to remain resonant in the over-tuning region.

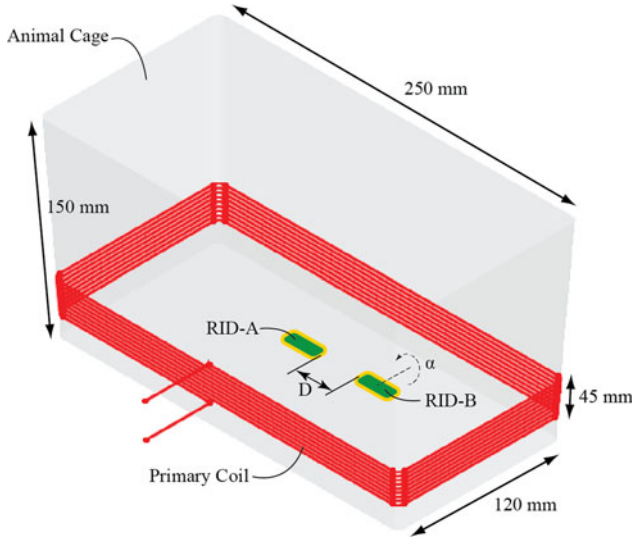

Fig. 14. WPT using multiple rodents in the same primary coil.

Experimental results with the CTD LCWPT system

The CTD LCWPT system was constructed and two main experiments were conducted to test its performance. In the first experiment, we simulated the mutual coupling effect by using two RID telemetric devices within the same primary coil (cage). In the second experiment, we tested the performance of the CTD control system to regulate the received power of the RID, as the RID rotates within the primary coil and automatically switches between different capacitor states based on its orientation. In all of the experiments, the performance of the CTD depends on four parameters: (1) the current applied to the primary coil, (2) the internal matched impedance (R_L) of the secondary circuit (RID), (3) the secondary coil orientation with respect to the x–y plane of the primary coil, and (4) the position of secondary coil inside the primary coil. For parameter (1) we applied a current (I_P) of 2 A (sinusoidal, peak-to-peak) to the primary coil for all experiments. For parameter (2) we used a secondary load R_L value of 10 kΩ for all experiments. For parameter (3), orientation was varied in both experiments by different means, as described in the following sections. For parameter (4) we placed the RID at the middle of the primary cage, because it represents the region of least electromagnetic flux density. For a rectangular primary coil, such as shown in Fig. 1, we have shown in previous work [3] that the flux density is highest in the corners, higher close to the edges, and is least density at the center of the cage.

We measured the power received by the RID using the WMS, where the WMS is only used for testing purposes. Since the WMS must provide reliable measurements over time, it is independently powered by a small lithium-polymer battery to make its operation independent of the secondary circuit performance [3–5, 40], as shown in Fig. 12. We used the WMS to measure the V_{rec} of the RID, and then we calculated the received power at the various orientations [3, 40]. The maximum power transferred was 180 mW when the RID is centered in the primary coil, and oriented parallel (0°) to the primary coil. The received power decreases as the orientation increases [3], where the received power at 30, 60, and 90° are 127, 38.2, and 3.5 mW, respectively.

Table 2. Measurements of V_{rec} and received power for fixed RID-A, for orientations 0 and 30° of RID-B

	RID-B at 0°		RID-B at 30°	
Dist. D (cm)	RID-A V_{rec} (V)	P (mW)	RID-A V_{rec} (V)	P (mW)
0	40.9	167	41.6	173
1	41.2	170	41.9	176
2	41.8	175	42.3	179
3	42.1	177	42.4	180
4	42.3	179	42.4	180
5	42.4	180	42.4	180
6	42.4	180	42.4	180

Table 3. Measurements of V_{rec} and received power for fixed RID-A, for orientations 60 and 90° of RID-B

	RID-B at 60°		RID-B at 90°	
Dist. D (cm)	RID-A V_{rec} (V)	P (mW)	RID-A V_{rec} (V)	P (mW)
0	41.9	176	42.2	178
1	42.2	178	42.4	180
2	42.4	180	42.4	180
3	42.4	180	42.4	180
4	42.4	180	42.4	180
5	42.4	180	42.4	180
6	42.4	180	42.4	180

Experimental results using multiple RIDs

To characterize the effect of mutual coupling between RIDs, an experiment with multiple RIDs in the same primary coil was conducted, as shown in Fig. 14. This helps to verify the capacitance needed to compensate for ΔL due to the mutual coupling between multiple RIDs. We used two RIDs within the primary coil, as shown in Fig. 14, which were attached to fixtures to mimic the positions and orientation of two mice. One RID denoted as RID-A was held stationary at 0° orientation at the center of the primary coil, while the other was moved by some distance with respect to it. The received power was measured on the stationary RID-A. The other moveable RID denoted as RID-B is placed at different positions away from the center, distance D, and is rotated by an angle α of 0, 30, 60, and 90°. The received power is a function of the orientation and distance between the two RIDs where the received power is calculated as V^2_{rec}/R_L (V_{rec} is measured when the I_P is 2 A, and R_L is 10 kΩ). Tables 2 and 3 list the values of measured V_{rec} and the calculated received power of RID-A. The maximum power variation is 7.5% when the moving RID-B is at the same orientation (0°) and 0 cm away (their edges touch each other) from the fixed RID-A, as shown in Table 2.

We measured the secondary inductance (L_{eqv}) using the HP 4285A LCR meter, when the two RIDs are at the same orientation and their edges touch each other. We found the ΔL equals to 1.2 μH. In order to tune the RID due to the ΔL, we used equation (8) to find the capacitance to be added/removed. This tuning capacitance is ~64 pF and could be used to compensate for the dropped power as a result of mutual coupling between multiple RIDs. In addition, the primary circuit needed adjusting for the variable capacitor (C_{par}) in the Class-E power amplifier, when the multiple RIDs are in the same cage (primary coil). The C_{par} was decreased/increased by a value of 3–8 pF. This small decrement/increment of the C_{par} was accomplished by a variable capacitor to achieve the magnetic resonant coupling between the primary circuit and the multiple RIDs (secondary circuits).

Experimental results of the CTD system at variable orientations

To test the performance of the CTD control system to regulate the received power of the RID, an experiment was done varying the RID orientation within the primary coil, allowing for observation of how the CTD system automatically switches between different capacitor states to vary its resonant frequency. We used a motorized system to vary the orientation of the RID, where the RID was mounted on a long plastic rod that protruded into the middle of the rodent cage (primary coil), with the other rod end connected to a programmable stepper motor. The motion profile for the orientation was developed to approximate a few typical orientations of a rodent's head during different activities and is illustrated in Fig. 15. Note that an orientation of 0° corresponds to the secondary coil in the RID being parallel to the x–y plane of the primary coil. For example, segment a to b corresponds to the RID rotating from 0 to +45°, segment e to f is rotation from 0 to −60°***, and segment g to h is rotation from −60 to +80°. The speed of the rotation was not observed to affect performance.

For this experiment, the RID was configured with two capacitors (C_{D1} and C_{D2}) for switching, allowing it to achieve four different values for total capacitance ($C_{D1} + C_{D2} + C_S$), as listed in Table 4. This gives the RID four distinct operation states: 0, 1, 2, and 3 based on the on/off states of C_{D1} and C_{D2}. Each state is associated with a specific resonant frequency of the RID, where state 3 represents a resonant frequency of 1 MHz, which matches the 1 MHz resonant frequency of the primary coil. In state 3, the maximum received voltage V_{rec} of 38.7 V is obtained when the RID is at 0° orientation.

For the purposes of this experiment, the MCU on board the RID was programmed to maintain received voltage V_{rec} within a range between 8 and 14 V. In practice, any voltage range can be designed for use, by selection of values of C_{D1} and C_{D2}, and the threshold values programmed in software. It is generally desirable to keep the received voltage V_{rec} on the DC side of the RID circuit within a voltage range that is suitable for application electronics. For example, CMOS logic devices are generally not suitable for voltages above 15–18 V, where in previous work voltage regulators were used to keep voltages at rated values, such as 10 V. However, a voltage regulator will dissipate excess voltage above its rated value as heat. In the current device, Fig. 16 illustrates how the received voltage V_{rec} varies for each of the 4 states of Table 4, as the orientation of the RID varies from 0 to 90°. Consider the situation when the RID is in state 3, which produces the strongest resonant coupling, and results in the maximum power transfer when the RID is oriented at 0°. If the RID remains at state 3 at 0° orientation, maximum V_{rec} will be ~38.7 V with a transferred power of 150 mW. As described in previous sections (Introduction) and (Methodology for control of tuning or detuning), the excess power must be dissipated which will result in very significant heating of the RID. However, if the RID could be in

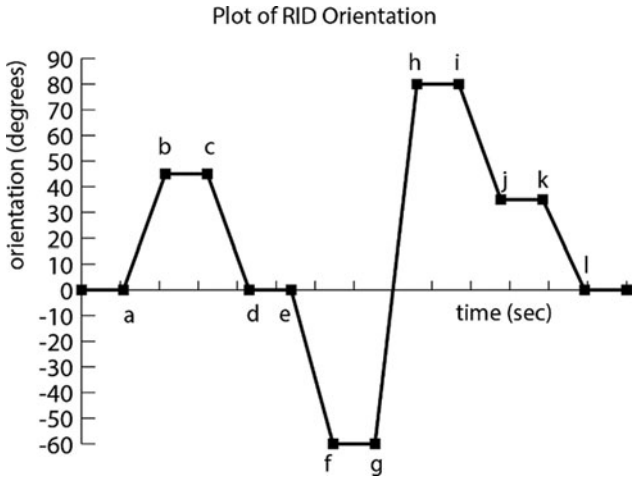

Fig. 15. Plot of RID orientation with respect to time, to simulate angles of rat's head.

Table 4. Capacitor values for CTD switching experiment

RID state	C_S 320 pF	C_{D1} 100 pF	C_{D2} 150 pF	V_{rec}^{a}(V)	P^{a} (mW)
3	–	On	On	38.7	150
1	–	On	Off	23.5	55
2	–	Off	On	33.5	112
0	–	Off	Off	13.5	18

[a]Values of V_{rec} and power correspond to 0° orientation of RID.

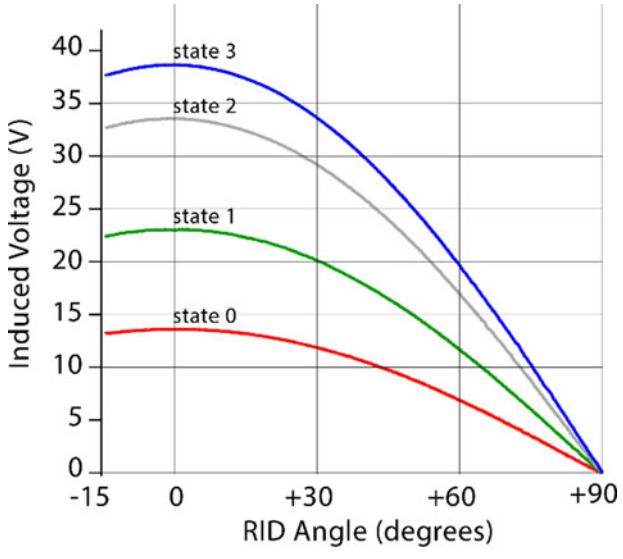

Fig. 16. Four operational states of RID showing V_{rec} versus orientation.

state 0 when it is oriented at 0°, the maximum V_{rec} would be ~13.5 V with a transferred power of 18 mW. If the application electronics only needs 10 V, this small excess voltage can be dissipated with very little excess heat. Therefore, when the RID is at ~0° orientation, it is desirable for it to be in the untuned state 0. As another example, consider the situation when the RID is in state 3 at a high rotation to the horizontal plane, of perhaps 65 to 80°. We can see from Fig. 16 that the state 3 received voltage at 65 to 80° will be ~15 to 5 V, which is a reasonable range for the application electronics. However, if the RID was in state 0 while oriented from 65 to 80°, its received voltage will be ~5 to 0 V, which is insufficient power for the application electronics. Therefore, when the RID is at 65 to 80° orientation, it should be in the best tuned state 3. It is the job of the CTD system to automatically switch between states 0, 1, 2, and 3, depending on the measured value of V_{rec}, to keep it in the range between 8 and 14 V.

The software code to control the on/off switching of capacitors C_{D1} and C_{D2} is illustrated as a flow chart in Fig. 17. The RID monitors V_{rec} every 40 ms and executes the decision logic shown. Upon power up of the RID, the CTD begins at the furthest untuned state, state 0 and enters the main loop, where it measures V_{rec}. If the system measures V_{rec} to be below V_{low} (i.e. 7.5 V), more power is needed to operate, so it will switch to state 1 by switching on capacitor C_{D1}, as shown in Table 4. Conversely, if it measures V_{rec} to be above V_{low}, it will remain in state 0, since it has adequate power to operate. The CTD system constantly keeps track of which state it is currently in, and whether or not it is within the desired voltage range (in this example between 7.5 and 14 V).

The performance of the CTD system was evaluated by running the RID through the motion profile illustrated in Fig. 15. The ability of the CTD to maintain the received voltage V_{rec} is illustrated in Fig. 18. Points *a* through *l* are noted, corresponding to the positions of the motion profile. The solid black line shows V_{rec} as the RID moves through the full profile, and it can be observed that it stays within the target range of 8 to 14 V, with the exception of the segment *h*–*i*. The RID begins at state 0 at 0° at point *a*, and then rotates to +45°, holds for 1 s, and then rotates back −45° to return to 0°, and holds for 1 s to reach point *e*. During this motion segment *a*–*e*, V_{rec} stays within 8 to 14 V, and hence no state change is triggered by the CTD. From point *e*, the RID then rotates to −60° and as it approaches point *f*, V_{rec} drops below 8 V and the CTD commands a state change to state 1, by turning on C_{D1}. This better tunes the RID to the primary coil, as shown by the V_{rec} values of Fig. 16 for state 1. Now being on the state 1 curve corresponding to 60° orientation, the V_{rec} value is constant while the motion profile pauses for 1 s, to reach point *g*. From points *g* to *h*, the RID rotates +140° in a continuous rotation. Soon thereafter, as it moves from −60° to ~ −55°, the V_{rec} value is measured to exceed 14 V, and the state is bumped down to state 0. As it proceeds to rotate, it eventually reaches 0° at state 0, as seen by the small hump, and continues with positive rotation. Figure 19 shows a close-up view in the vicinity of segment *h*–*i*. As the RID rotates it reaches +55° orientation, where V_{rec} drops below 8 V and it switches to state 1. Shortly thereafter, as the RID reaches +70° orientation, V_{rec} again drops below 8 V and it switches to state 2. Shortly thereafter, the RID reaches +75° orientation, and V_{rec} again drops below 8 V and it switches to state 3 (the best coupling state). Very soon thereafter, the orientation of the RID becomes 80° (point *h*), however it is already at its best coupling state 3 and V_{rec} drops to about 4 V.

On the return path, starting at point *i*, the RID beings a −45° rotation. Being in state 3, as it reaches +75° orientation, and V_{rec} increases to beyond 14 V, and it switches to state 2. Shortly thereafter, the RID reaches +70° orientation, V_{rec} increases to beyond 14 V, and it switches to state 1. With further rotation it reaches +55° orientation, V_{rec} increases beyond 14 V, and it switches to state 0. It remains in state 0 until it reaches +35° orientation at point *j*. The motion profile is completed with a final rotation to

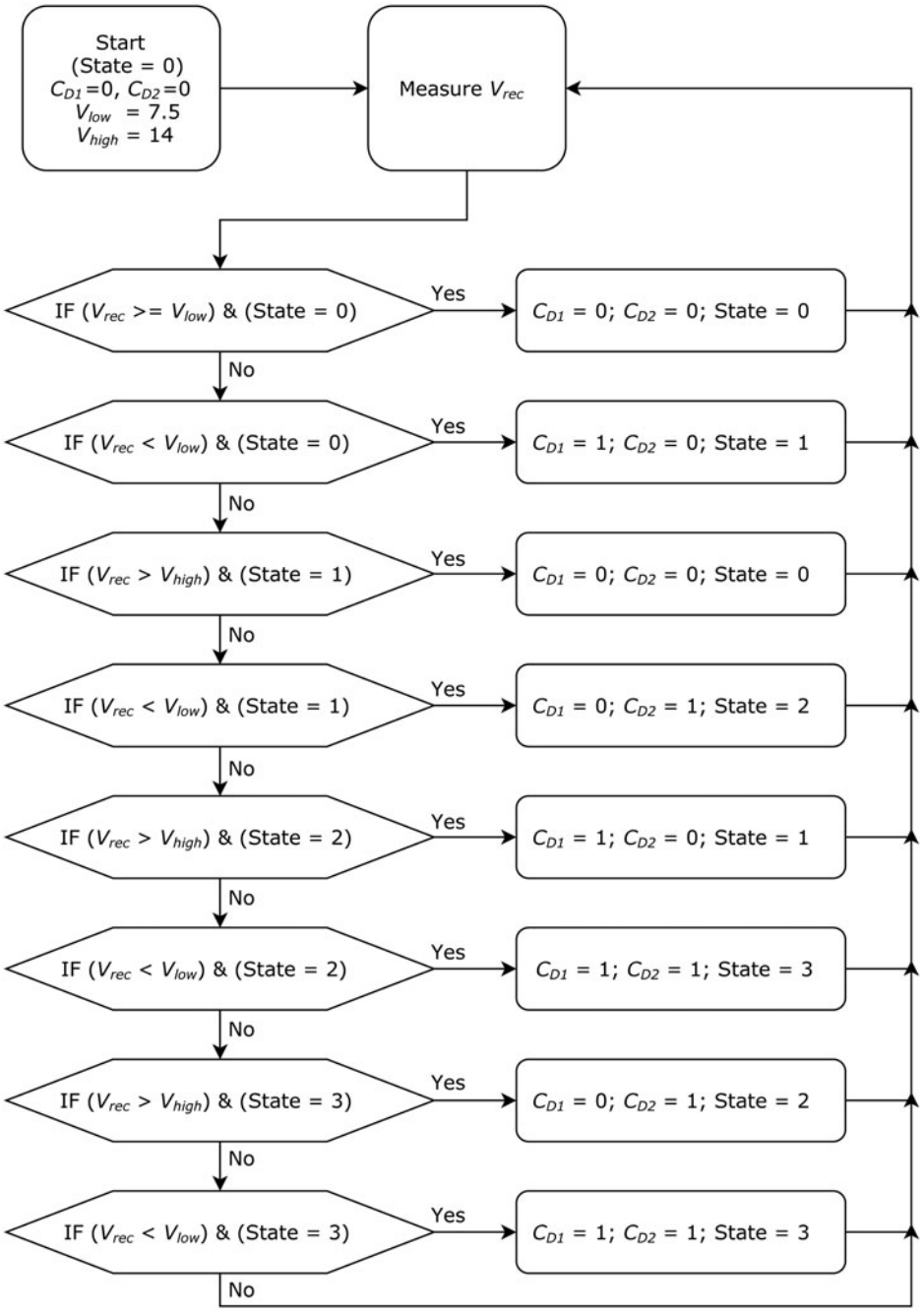

Fig. 17. Flow chart of control code for the CTD algorithm.

0° orientation at point *l*, as shown in Fig. 18. All the recorded data shown in Figs 16, 18 and 19 was collected by the WMS, which communicates wirelessly via a radio link to the base station, which is in turn connected to a laptop that collects the data live. There is no data storage onboard the RID for these experiments.

Discussion

In the mutual coupling experiment, we observed that mutual coupling occurs between multiple secondary coils, however, the effect was minor. The mutual coupling can detune the resonant frequency of the secondary circuit by 5–20 kHz. As a result of this resonant frequency mismatch, the received power by the secondary circuit drops slightly [8]. For example, the maximum reduction of the received power is 7.5% when the edges of the two secondary circuits touch each other at the same orientation, as shown in Tables 2 and 3. Also, it was noted that the resonance of the primary circuit detunes by 10 kHz, when multiple (two) secondary circuits are used in the same primary coil.

In the experiment to evaluate the CTD system switching performance, we observed good performance of the system. By using two different capacitors C_{D1} and C_{D2} for on/off switching along with C_S, the system was able to achieve four different states (i.e. four different resonant frequencies of the secondary circuit), where one of those states (state 3) matched the resonant frequency of the primary circuit. The performance of each state is shown in Fig. 16, and ideally each state curve should be spaced evenly from adjacent curves. However, given the system complexity (all component values work together to influence the resonant frequency)

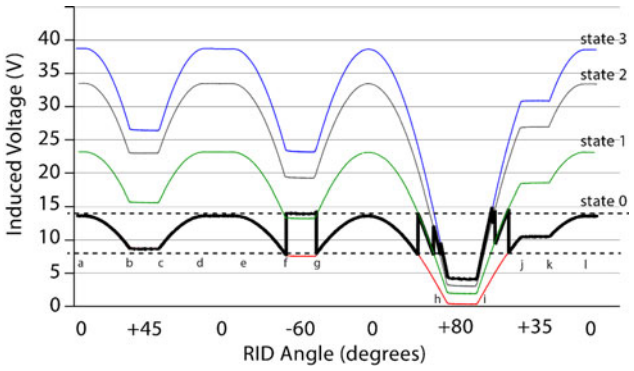

Fig. 18. Performance of CTD system switching between four states of the RID, showing V_{rec} versus orientation.

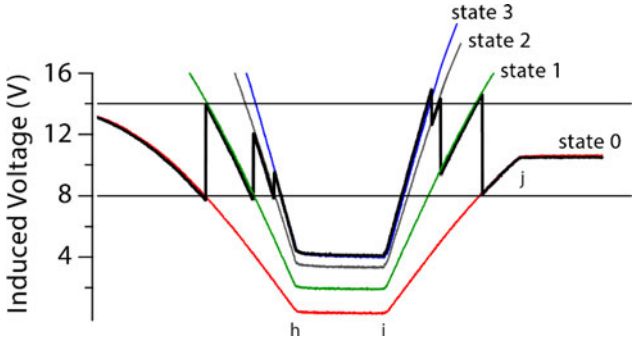

Fig. 19. Close-up of CTD system switching between four states in vicinity of segments *h–i*.

and capacitor availability, the curves as shown were able to demonstrate the CTD switching concept.

In future, temperature sensors (thermistors) could be used and connected with the free ADC channels of the MCU to measure and monitor the temperature of the RIDs. Moreover, a system with four different capacitors, could achieve 16 possible states, for much finer tuning and detuning of the secondary circuit from the primary. Hence, our CTD scheme can be considered as a coarse tuning/detuning of the resonance of the secondary circuit, which has an advantage point of a low switching loss from the MOSFETs. To sum up, the CTD can regulate the induced voltage/received power of the RID, without high power voltage regulators or power electronics and thereby avoid significant on-board generation of heat which may damage the implant.

Conclusion

This paper reported reasons that cause resonant frequency mismatch between the primary circuit and multiple secondary circuits in WPT systems. A literature review shows how various researchers address the resonant frequency mismatch in WPT systems. Researchers used two schemes to control magnetic resonant coupling of WPT systems, which are controlling the resonance of the primary coil or the secondary coils. Controlling the primary circuit is not suitable for our application, which requires powering of multiple secondary coils (RIDs). For the use of freely moving multiple secondary coils (RIDs) within the same stationary primary coil, controlling the resonance of the secondary circuits is a suitable technique. Different initial schematics of controllable RID were built to tune/detune its resonance, and initial versions did not work properly because of the floating gate drive problem in the L_SC_S-tank circuit. This gate drive problem was solved using the voltage doubler circuit, shown in Fig. 10. The resonance of the secondary circuit was controlled by adding a bank of capacitors (C_{D^*}) that are on/off switchable, into the L_SC_S-tank circuit. Switching of the capacitors was achieved using MOSFETs, directly connected to the on-board MCU. The on-board MCU runs a control program (Fig. 17) and is actively measuring V_{rec}. An experimental setup with two secondary circuits (RIDs) was conducted to investigate the mutual coupling effect between the RIDs. The experimental results showed that the maximum drop of the received power is 7.5%, when the edges of the two RIDs touch each other, which does not present a problem for powering the RID. A second experiment to evaluate the performance of the new CTD system was done. The purpose was to actively tune/detune the RID to prevent on-board temperature rise due to excessive transferred power when the RID is strongly coupled to the primary circuit. The results showed good performance of the CTD system. The CTD was able to detune the resonance of the secondary circuit, when secondary coil voltage is higher than a defined limit or tune the resonance of the secondary when voltage is lower than a defined limit.

References

1. **Poon ADY** (2014) *Miniaturization of Implantable Wireless Power Receiver*. Implantable Bioelectronics, Weinheim, Germany: Wiley, ch. 4, pp. 45–64, March 2014.
2. **Si P, Hu AP, Hsu JW, Chiang M, Wang Y, Malpas S and Budgett D** (2007) Wireless power supply for implantable biomedical device based on primary input voltage regulation, in 2nd *IEEE ICIEA*, 2007, pp. 235–239.
3. **Badr BM, Somogyi-Gsizmazia R, Delaney KR and Dechev N** (2015) Wireless power transfer for telemetric devices with variable orientation, for small rodent behavior monitoring. *IEEE Sensors Journal* **15**, 2144–2156.
4. **Badr BM, Somogyi-Csizmazia R, Delaney KR and Dechev N.** Maximizing wireless power transfer using ferrite rods within telemetric devices for rodents, in *COMSOL Conference*, Boston, USA, Oct. 7–9.
5. **Badr BM, Somogyi-Csizmazia R, Dechev N and Delaney KR** (2014) Power transfer via magnetic resonant coupling for implantable mice telemetry device, in *Proc. IEEE WPTC*, Jeju, South Korea, May 8–9, pp. 259–264.
6. **DeMichele GA and Troyk PR** (2003) Integrated multi-channel wireless biotelemetry system, in 25th *IEEE EMBS*, pp. 3372–3375.
7. **McCormick D, Hu AP, Nielsen P, Malpas S and Budgett D** (2007) Powering implantable telemetry devices from localized magnetic fields, in *IEEE EMBS*, pp. 2331–2335.
8. **Wang C-S, Stielau OH and Covic GA** (2000) Load models and their application in the design of loosely coupled inductive power transfer systems, in *IEEE PowerCon Conference*, pp. 1053–1058.
9. **Cannon BL, Hoburg JF, Stancil DD and Goldstein SC** (2015) Magnetic resonant coupling as a potential means for wireless power transfer to multiple small receivers. *IEEE Transactions on Power Electronics* **24**, 1819–1825.
10. **Badr BM** (2016) *Wireless Power Transfer for Implantable Biomedical Devices Using Adjustable Magnetic Resonance* (Ph.D. dissertation). Department of Mechanical Engineering, University of Victoria, BC, Canada.
11. **Wireless Battery Charging, (2019, Jan. 16).** [Online]. Available at www.st.com.
12. **Exploring the evolution and optimization of wireless power transfer, (2019, Jan. 16).** [Online]. Available at www.ti.com.
13. **Dissanayake TD, Budgett DM, Hu P, Bennet L, Payner S, Booth L, Amirapu S, Wu Y and Malpas SC** (2010) A novel low temperature

transcutaneous energy transfer system suitable for high power implantable medical devices: performance and validation in sheep. *Artificial Organs* **34**, 160–167.
14. **Ng DC, Bai S, Yang J, Tran N and Skafida E** (2005) Wireless technologies for closed-loop retinal prostheses. *Journal of Neural Engineering* **6**, 1–10.
15. **Brusamarello VJ, Blauth YB, Azambuja RD, Muller I and Sousa FRD** (2013) Power transfer with an inductive link and wireless tuning. *IEEE Transactions on and Instrumentation and Measurement* **62**, 924–931.
16. **Si P, Hu AP, Malpas S and Budgett D** (2008) A frequency control method for regulating wireless power to implantable devices. *IEEE Transactions on Biomedical Circuits and Systems* **2**, 22–29.
17. **James J, Boys J and Covic G** (2005) A variable inductor based tuning method for ICPT pickups, in 7th *IEEE IPEC Conference*, pp. 1142–1146.
18. **Si P, Hu AP, Malpas S and Budgett D** (2006) Switching frequency analysis of dynamically detuned ICPT power pick-ups, in *IEEE PowerCon Conference*, pp. 1–8.
19. **Hsu J-UW, Hu AP and Swain A** (2009) A wireless power pickup based on directional tuning control of magnetic amplifier. *IEEE Transactions on Industrial Electronics* **56**, 2771–2781.
20. **Hsu J-UW, Hu AP and Swain A.** Fuzzy based directional tuning controller for a wireless power pick-up, in 10th *IEEE TENCON Conference*, 2008, pp. 1–6.
21. **Covic GA, Boys JT and Peng JC-H** (2008) Self tuning pick-ups for inductive power transfer, in *Power Electronics Specialists Conference*, pp. 3489–3494.
22. **Huang C-Y, Boys JT, Covic GA and Ren S** (2010) LCL pick-up circulating current controller for inductive power transfer systems, in *Energy Conversion Congress and Exposition*, pp. 640–646.
23. **Hsu J-UW, Swain A and Hu AP** (2001) Implicit adaptive controller for wireless power pickups, in *Industrial Electronics and Applications Conference*, pp. 514–519.
24. **Hsu J-UW, Hu AP and Swain A** (2012) Fuzzy logic-based directional full-range tuning control of wireless power pickups. *IET Power Electronics*, **5**, 773–781.
25. **Pantic Z** (2013) *Inductive Power Transfer Systems for Charging of Electric Vehicles* (Ph.D. thesis). Department of Electrical Engineering, North Carolina State University, Raleigh, North Carolina.
26. **Petersen E** (2015) Variable capacitor for resonant power transfer systems. *US patent number WO2014018968 A2*, July 2015.
27. **Riehl PS, Satyamoorthy A and Akram H** (2014) Open-circuit impedance control of a resonant wireless power receiver for voltage limiting. *US patent number WO2014052686 A2*, Sep. 2014.
28. **Yen Y-C, Riehl PS, Akram H and Satyamoorthy A** (2015) Wireless power receiver with programmable power path. *US patent number WO2015105924 A1*, July 2015.
29. **Fleisch D** (2008) *A Student's Guide to Maxwell's Equations*. Cambridge, UK: Cambridge University press.
30. **Yang Z, Liu W and Basham E** (2007) Inductor modeling in wireless links for implantable electronics. *IEEE Transactions on Magnetics* **43**, 3851–3860.
31. **Xue R-F, Cheng K-W and Je M** (2013) High-efficiency wireless power transfer for biomedical implants by optimal resonant load transformation. *IEEE Transactions on Circuits and Systems I: Regular Papers* **60**, 867–874.
32. **Application note "Comparison of ceramic and tantalum capacitors" (2015, June 16).** [Online]. Available at www. Kemet.com.
33. **Microcontroller Nordic "nRF24LE1-F16Q48, Ultra-low Power Wireless System" (2015, June 16).** [Online]. Available at www.nordicsemi.com.
34. **Wang C-S, Stielau OH and Covic GA** (2005) Design considerations for a contactless electric vehicle battery charger. *IEEE Transactions on Industrial Electronics* **52**, 1308–1314.
35. **Boys JT, Covic GA and Xu Y** (2003) DC analysis technique for inductive power transfer pick-ups. *IEEE Power Electronics Letters* **1**, 51–53.
36. **Yu Q, Holmes TW and Naishadham K** (2002) RF equivalent circuit modeling of ferrite-core inductors and characterization of core materials. *IEEE Transaction on Electromagnetic Compatibility* **44**, 258–262.
37. **Green L** (2001) RF-inductor modeling for the 21st century. *Designfeature*, 67–74. Available at https://scholar.google.com/scholar_lookup?hl=en&publication_year=2001&pages=67-68&author=L.+Green&title=%E2%80%98RF-Inductor+Modeling+for+the+21st+Century%E2%80%99
38. **Gate driver "MIC4421" (2019, Jan. 16).** [Online]. Available at http://www.micrel.com.
39. **MOSFET "IRF840" (2019, Jan. 16).** [Online]. Available at http://www.vishay.com.
40. **Badr BM, Somogyi-Csizmazia R, Leslie P, Delaney KR and Dechev N** (2016) Design of a wireless measurement system for use in wireless power transfer applications for implants. *Journal of Wireless Power Transfer* **4**, 21–32.
41. **Sokal NO and Sokal AD** (1975) Class E-A new class of high-efficiency tuned single-ended switching power amplifiers. *IEEE Journal of Solid-State Circuits* **10**, 168–176.
42. **Sokal NO and Sokal AD** (1975) High-efficiency tuned switching power amplifier. *USA Patent number 3,919,656*.
43. **Sokal NO** (1981) Class E high-efficiency switching-mode tuned power amplifier with only one inductor and one capacitor in load network-approximate analysis. *IEEE Journal of Solid-State Circuits* **16**, 380–384.

Basem M. Badr received B.Sc. in Electrical and Power Systems from Mansoura University, Egypt in 2007, and the Master's degree in Control Systems Engineering from King Saud University, Saudi Arabia in March 2011. He had the Ph.D. degree in Mechanical Engineering at the University of Victoria, in 2016. He is an accomplished book author, hold three patents and had many journal and conference papers. His research interests include Wireless Power Transfer, Energy Harvesting, Biomedical Applications, Control Systems, and Electric Motor Drives. His industry work experience spans the biomedical and renewable energy sectors.

Art Makosinski holds a BA in Industrial Education from Newark State College/Newark College of Engineering in 1973. He has been Manager of Laboratories at the Department of Mechanical Engineering at the University of Victoria between 1988–2017 and 2018–2019. He has coauthored several patents in the fields of energy conversion and medical sensors. His current work is focused on the design and construction of ultra-low power converters and archival film scanning methods.

Nikolai Dechev received his B.A.Sc., M.A.Sc., and Ph.D. degrees from the Department of Mechanical Engineering, University of Toronto, in 1996, 1999, and 2004, respectively. He is currently an Associate Professor and Department Chair of Mechanical Engineering at the University of Victoria, Canada. His research program centers on biomedical systems design in the area of hand prosthesis. This involves aspects such as bio-signal measurements, implantable sensors and prosthesis control. He also has expertise in MEMS sensors, and robotic micromanipulation. Dr. Dechev is a Member of the IEEE.

Kerry R. Delaney received his BSc in zoology from the University of British Columbia and Ph.D. in neuroscience from Princeton University, Princeton NJ in 1987. Next he undertook post-doctoral work in neuroscience at U.C. Berkeley, New York University and AT&T Bell laboratories before being appointed to the faculty at Simon Fraser University, BC in 1992. He joined the faculty at the University of Victoria in 2004 and is currently Professor of Biology, and former Chair of the Department. His research program focuses on synaptic and cellular neurophysiology of olfactory sensory processing, neuromuscular transmission, and the role of synaptic dysfunction in neuro-developmental disorders such as Rett syndrome, using a variety of optical and electrophysiological techniques. See web.uvic.ca/delaneylab for more information.